Title

Laurdan Identifies Different Lipid Membranes in Eukaryotic Cells

Permalink

https://escholarship.org/uc/item/9m80z238

ISBN

978-1-4822-0989-1

Authors

Gratton, Enrico
Digman, Michelle A

Publication Date

2015

DOI

10.1201/b17634

Copyright Information

Peer reviewed

13 Laurdan Identifies Different Lipid Membranes in Eukaryotic Cells

Enrico Gratton and Michelle A. Digman

CONTENTS

13.1 INTRODUCTION

13.1.1 SPECTROSCOPIC PROPERTIES OF LAURDAN

There are several commonly used approaches for the study of membrane properties of live cells based on fluorescence probes. In one approach, lipids with specific fluorescent markers are incorporated in the cell membranes. The advantage of this approach is that it is possible to study the membrane distribution of specific lipids. However, when the aim of the study is to detect membrane microdomains independently of their

lipid composition, it is more useful to use a single probe that can report on the specific properties of the membrane microdomains, independently of the probe segregation in one specific domain and location in the cell. One fluorescent probe that has been successfully used for this purpose is the lipophilic probe Laurdan (2-dimethylamino-6-lauroylnaphthalene), originally synthesized by Weber and Farris.[1] Different membrane environments produce marked changes both in the spectrum and in the fluorescence lifetime of Laurdan. The sensitivity of the emission spectrum of Laurdan to the environment originates from the specific molecular structure of Laurdan in which the excited-state dipole is substantially different from the ground-state dipole (Figure 13.1).

During the absorption of the excitation photon, which lasts approximately 10^{-15} s, there is no time for reorientation of the surrounding solvent molecules, generally water in biological samples (Figure 13.2).

Depending on the nature of the environment, the reorientation of solvent molecules around the excited-state dipole of Laurdan can occur in the nanosecond time range. This time is comparable to the total duration of the excited state and, as a consequence of the solvent reorientation, the spectrum of Laurdan changes with time after excitation in a continuous way (Figure 13.3).

This property of Laurdan, which results in an "undefined" emission spectrum, since the spectrum depends on the time after excitation, must be considered with extreme care when we want to identify the emission with a particular "phase" of structural organization of the membrane. Originally, our laboratory proposed using a specific scale, the Generalized Polarization (GP) scale to quantify the degree of dipolar relaxation.[2–4] This scale is experimentally defined using the emission spectral bandwidths and measuring the normalized emission in the two bandwidths. Specifically, the two bandwidths were chosen at 440/20 nm and 490/20 nm and the GP value is calculated according to the following expression:

Time-dependent spectral relaxations

Solvent dipolar orientation relaxation

10^{-15} s 10^{-9} s

Ground state   Franck–Condon state   Relaxed state

Immediately after excitation   Long time after excitation

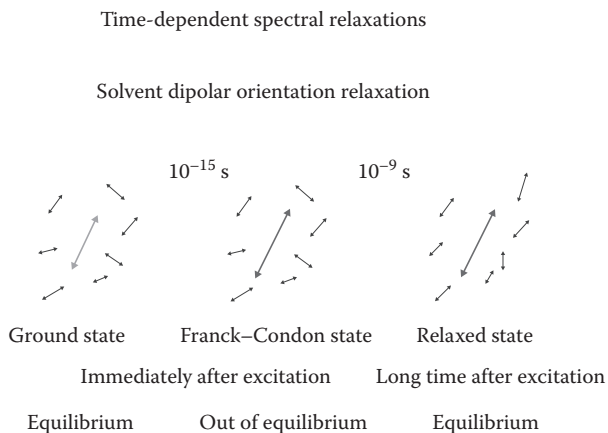Equilibrium   Out of equilibrium   Equilibrium

FIGURE 13.1 In the ground state, solvent molecules are partially organized around the Laurdan molecule. Upon excitation, which occurs in 10^{-15} s, the Laurdan dipole substantially increases. At this point in time, the solvent molecules start to rotate to minimize the energy with respect to the excited-state dipole until equilibrium is reached.

As the relaxation proceeds, the energy of the excited state decreases
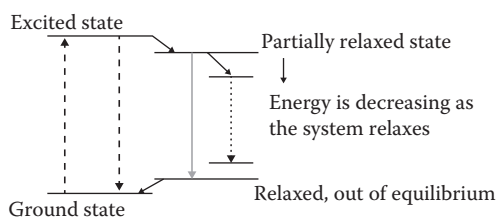and the emission moves toward the dotted vertical transition

FIGURE 13.2   Jablonski diagram indicating the relative position of the excited state at the time
of excitation and the shift of the level of the excited state as the energy is minimized as a result of
the orientation of the solvent molecules. The colors of the different down arrows schematically
show that the energy of the emitted photon decreases as a function of time after excitation.

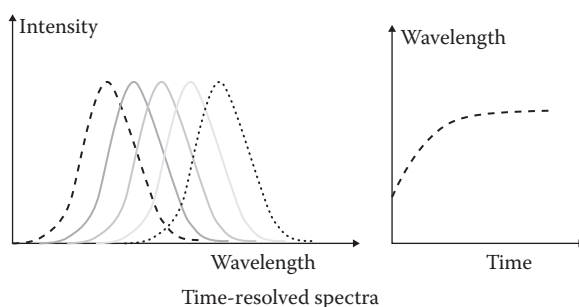The emission spectrum moves toward the dotted vertical transition with time

FIGURE 13.3   Schematic representation of the continuous shift of the wavelength of emis-
sion of the fluorescence. The first molecules to decay emit in the dashed line and the last ones
emit in the dotted line. The apparent lifetime of the excited state changes with time. If one is to
measure using a bandpass in the dotted part of the spectrum, initially there is no emission in this
bandpass since the spectrum has not shifted yet. In the dotted part of the spectrum, the intensity
starts to increase after some time and then eventually decays to zero. This delay of the emission
gives rise to a very peculiar behavior of the apparent lifetime in the dotted part of the spectrum.

$$GP = \frac{(I_{440} - gI_{490})}{(I_{440} + gI_{490})}. \qquad (13.1)$$

Note that the intensity in the two filters must be calibrated for each instrument
and for a specific set of filters since the sensitivity of the instrument could be dif-
ferent from one laboratory to another. This is done by determining the value of the
constant g in Equation 13.1 using as compound of known GP, generally Laurdan
in dimethyl sulfoxide (DMSO). Note also that given the definition, the GP value is
constrained to be between +1 and −1. While the GP is rigorously defined, the mean-
ing of the GP must be carefully discussed. There is a general trend of the values of

the GP that is very useful for the evaluation of the membrane overall properties. For example, when the dipolar relaxations are slow compared to the excited-state lifetime, most of the emission occurs in the 440 nm filter (blue filter) and the GP is positive and typically in the range 0.6 to 0.7. When the dipolar relaxations are fast (compared to the excited-state lifetime), most of the emission is in the 490 nm filter (green filter) and the GP is negative in the −0.3 range.

What is important for the discussion here is that, in principle, there are no definite values for the GP in different membrane phases since the rate of dipolar relaxation is strongly influenced by the lipid composition, membrane curvature, presence of defects, and other parameters than can affect the rate of dipolar relaxation as well as the duration of the excited-state lifetime. For example, if the excited-state lifetime is shortened because of quenching effects, the GP will increase without a change of the dipolar relaxation rate. Specifically, depending on the polarity of the solvent, the excited-state lifetime can change. In apolar solvents, the fluorescence lifetime of Laurdan can be in the range 7–8 ns, while in more polar solvents, the lifetime can be in the range 3–4 ns. Hence, by a mere change of the polarity of the membrane, the GP value can change by a relatively large factor without a corresponding change in the rate of dipolar relaxation. One notable example is the presence of cholesterol in the membrane, which increases the lifetime of Laurdan, allowing for more time for the dipolar relaxation to occur. From this discussion, it is clear that the measurement of Laurdan lifetime provides complementary information needed to properly interpret the spectral changes. Also, it is clear that the assumption that there are only two values for the Laurdan GP (or lifetime) must be carefully discussed and probed. Mainly for this reason, the GP function was initially proposed as an index that correlates with the water content of the membrane to be used to detect changes in membrane packing that influence the amount of water in the membrane.

As laser scanning fluorescence microscopy was developed in the 1990s and with the advent of femtosecond lasers that allowed two-photon excitation of Laurdan, we were able to obtain images of GP that clearly show that the GP function is different in different cells and in different membranes or part of the same membrane of the cell.[5] Then, an important issue arose about the meaning of the absolute value of the GP and whether this value could provide information about membrane composition and membrane packing. Although we could measure the entire emission spectrum and the lifetime in each emission bandwidth in a bulk experiment, this is more complicated in the microscope setup. Most of the earlier studies were done using two emission bandpasses (generally referred to as the blue and green filters) and the GP function was calculated at each pixel of the image.[2] The GP scale was used to interpret the GP "image" as regions in the cell in which the membrane was more or less permeable to water. This approach provided interesting results, and it was used mainly for producing contrast in images on the basis of the GP value.[6] The question that will be discussed next is if we could assign values of the GP to specific membrane phases such as highly packed liquid ordered phase and less packed liquid disordered phase. Since we want to fabricate a scale to determine the correlation between the Laurdan emission spectrum and the phase of the membrane, we should look at the entire emission spectrum and possibly perform lifetime measurements at selected bandpasses in the microscope setup. We also need to find a way to visualize all this information (spectrum and lifetime) in

such a way that we could correlate the pixel histogram of the GP values with a specific structure in the image. Note that this procedure is different from using a fluorescent label that partitions in a specific lipid structure or cell organelle.

13.2   THE PHASOR APPROACH TO SPECTRAL AND LIFETIME ANALYSIS

For this discussion, we have developed an approach that is based on the measurement of the spectrum of Laurdan obtained in a microscope setup where a single giant unilamellar vesicle (GUV) or cell can be visualized and analyzed. As we discussed, the spectrum changes continuously in time as the excited state returns to the ground state. We are using an analysis based on the "phasor approach" in which the spectrum is characterized by a few parameters. The advantage of the phasor approach is that we can represent some spectral characteristics in a global view in the phasor plot. Another advantage is that if there are only two (or a few) discrete spectra that are typical of a type of membrane domain, then it will be possible to distinguish the combination of domains containing regions with characteristic spectra because the phasor components add linearly for two (or more) species.[7–9] Given a spectrum measured at each pixel indicated by $I(\lambda)$, according to Fereidouni et al.,[10] we define the following two quantities that we interpret as two coordinates in a Cartesian plot. The symbol n indicate the "harmonic order" and we use generally either a value of 1 (first harmonic) or 2 (for the second harmonic) for n.

$$g = \frac{\sum_{\lambda} I(\lambda)\cos(2\pi_n\lambda/L)}{\sum_{\lambda} I(\lambda)} \quad s = \frac{\sum_{\lambda} I(\lambda)\sin(2\pi_n\lambda/L)}{\sum_{\lambda} I(\lambda)} \tag{13.2}$$

A typical spectrum for Laurdan in the laser scanning microscope Zeiss 710NLO is shown in Figure 13.4, using two-photon excitation at 790 nm.

Unfortunately, given the limited range of the spectral detectors for commercial microscopes, we are generally limited to collect only a portion of the emission spectrum. Clearly, in the spectrum of Figure 13.4, we are cutting all the emissions below 416 nm. This is not a limitation since the g and s functions are defined only in the region of the measurement (Equation 13.2). A fundamental property of the coordinates g and s is that they behave as components of a vector. That means that if the measured spectrum is the sum of two spectra, the measured g and s are the sum of individual coordinates for each of the spectra measured independently. This is illustrated in Figure 13.5 where the phasor positions for two spectra are schematically shown with the black and gray dot. Figure 13.5 shows that the position of a phasor is determined by the phase angle and the modulus, that is, the radial position of the phasor. In Figure 13.5, the angular position in the phasor plot (counterclockwise) corresponds to the average wavelength of emission where bluer emissions have smaller phases. The radial distance from the center depends on the spectrum width with narrower spectra having larger radii. The harmonic number $n = 2$ multiplies the phases
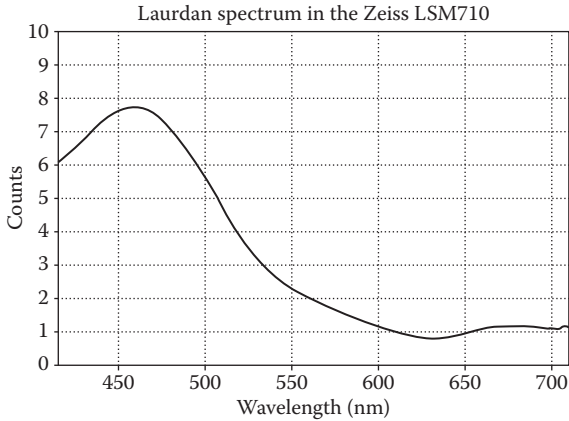
FIGURE 13.4 Typical spectrum of Laurdan in cells measured using the spectral detector of the Zeiss LSM710 laser scanning microscope. The spectrum is obtained using two-photon excitation at 790 nm. The spectral detector has 32 independent detectors equally spaced in wavelength in the region 416 to 727 nm. In this figure, the intensity of the detectors is interpolated and the spectrum is smoothed.
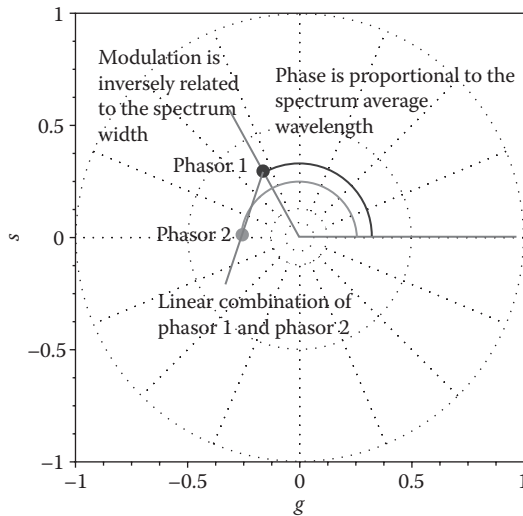
FIGURE 13.5 Spectral phasor plot indicating the position of the phasor corresponding to two different spectra. The angular position of a spectrum in the phasor plot is proportional to the average emission wavelength while the radial potion is inversely related to the spectral width. If in a pixel we have the combination of the two spectra, the phasor position must fall in the line joining the phasor of the two spectra as indicated in the figure.

approximately by a factor of 2, and it is much less sensitive to the lack of cutoff of the spectrum owing to the limited wavelength range of the microscope and more sensitive to spectral changes. In this chapter, we use $n = 2$ for all spectral analysis.

For example, if a spectrum has a shape indicated by the dot 1 and another spectrum has the shape indicated by 2, their linear combination must follow the line joining the phasor plot of the phasors of the two spectra. The assessment whether or not a spectrum is the linear combination of 2 "unknown" spectra can be made without any knowledge of the spectra.

In principle, the spectral phasor analysis is equivalent to spectral demixing. However, in spectral demixing, we need to know the basis spectra used in the demixing algorithm, which are unknown for Laurdan. More importantly, the spectra change continuously because of solvent dipolar relaxations so that any method that assumes that there are only few spectral components is inadequate.

For the lifetime analysis, the phasor approach works in the same way as that for spectral analysis with some interesting additions as explained in Section 13.3.

13.3 THE LIFETIME PHASOR TRANSFORMATION AND ITS INTERPRETATION

In a fluorescence lifetime imaging microscopy (FLIM) measurement, the fluorescence decay is obtained at each pixel generally using a photon counting system that measures the histograms of time delays between the excitation of the molecule caused by the laser pulse excitation and the emission of a photon from the excited state of the molecule. In each pixel, an average of approximately 100 to 500 photons is collected. Analysis of the decay using exponential models cannot be done accurately using such a low number of photons in the histogram, and specifically for Laurdan, as discussed in Section 13.1, an exponential decay is inadequate to describe the decay since Laurdan decay is affected by solvent relaxations. In the phasor approach, only a few moments of the delay histogram are used to determine some proprieties of the decay. The phasor approach applies a transformation (the phasor transformation) to the measured decay histogram as shown in Equations 13.3 and 13.4, where $I_{i,j}(t)$ is the histogram of photon delays measured at pixel (i,j).[7] At each pixel, the phasor transformation provides two coordinates g and s, which are plotted in a polar plot called the phasor plot.

$$g_{i,j}(\omega) = \frac{\int_0^T I_{i,j}(t)\cos(\omega t)\mathrm{d}t}{\int_0^T I_{i,j}(t)\mathrm{d}t} \tag{13.3}$$

$$s_{i,j}(\omega) = \frac{\int_0^T I_{i,j}(t)\sin(\omega t)\mathrm{d}t}{\int_0^T I_{i,j}(t)\mathrm{d}t} \tag{13.4}$$

There is a relationship between the exponential decay and points in the phasor plot (Figure 13.6). If the fluorescence decay is single exponential, the phasor transformation gives points that lay on a semicircle called the universal circle.

As we indicated earlier, the phasor transformation has the property that the coordinates g and s behave like coordinates of a vector. The consequence of this mathematical property is that if in a pixel we have molecules that decay with two different exponential constants, the phasor of each of the molecules will lay on different points on the universal circle, but their linear combination (which depends on their fractional intensity contribution to the decay in that pixel) must be on the line joining the two points on the universal circle, as shown in Figure 13.7a. This linear combination property holds even if the phasors of the two species are not on the universal circle (Figure 13.7b). Since the decay of Laurdan is nonexponential, if in one pixel we have coexistence of regions of different decay properties, the measured phasor must be on the line corresponding to these different decay properties. For example, if in one pixel we have coexistence of regions (microdomains below the pixel resolution) of
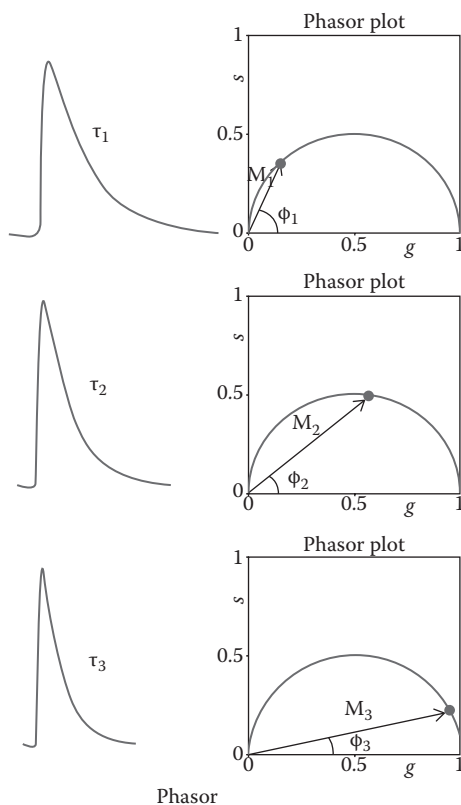

FIGURE 13.6   Schematic of the phasor transformation. Decay curves with different single-exponential lifetimes map in different position in the phasor plot with points on the universal circle. The faster is the exponential decay, the more the point is to the right.
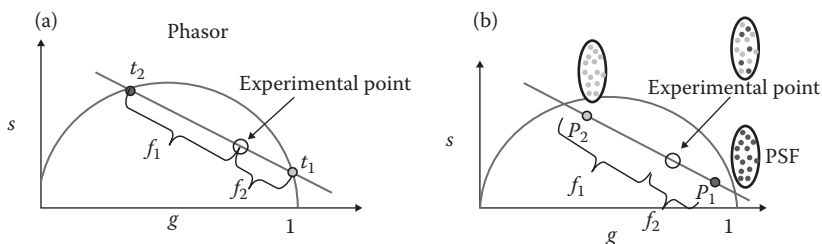
FIGURE 13.7   Linear combination property of phasors. (a) The combination in one pixel of two single exponentials gives a phasor value on the line joining the phasors corresponding to the two exponentials. (b) If in one pixel (the size of the PSF, approximately 300 nm) there are Laurdan molecules with different environments, although each environment is decaying as a complex exponential, they will combine linearly to give experimental points in the line joining the phasors of the two different environments.

liquid order and liquid disorder, then the phasor position must be along the line joining the phasor of the liquid ordered and liquid disordered membrane phases.

13.4   RESULTS OF THE ANALYSIS OF THE EMISSION OF LAURDAN USING SPECTRAL AND LIFETIME PHASORS IN GUVs MODEL SYSTEMS

We will first discuss the values of the spectral and lifetime phasors measured in GUVs composed of one lipid species (DPPC, DMPC, and DLPC).

Notably, the phasor values of the different composition and temperature GUVs follow a straight line. The colors of the circles in the phasor plot correspond to the colors in the images. As expected, Laurdan in DPPC at 20°C (T_m approximately at 41°C) is emitting in the blue (smaller phase), while Laurdan in DLPC at 20°C (T_m approximately at 8°C) has a spectrum that is in the green region (larger phase). The phasor positions of the samples at equal temperature (DPPC, DMPC, and DLPC) span a relatively large range in the phasor plot (red circle = 454 nm, green circle = 458 nm, cyan circle = 468 nm, blue circle = 480 nm). Surprisingly, the distance of the various phasor clusters from the origin varies. This distance is inversely related to the width of the spectrum, which is evidently different in the different samples. According to the linear combination rule for phasors, the samples that are in the linear segment in Figure 13.8 (not at the extreme of the segment) should contain a linear combination of the spectral properties corresponding to the extremes of the segment. For example, the cluster of phasors indicated with the color green or cyan should correspond to the linear combination of the two spectra corresponding to the red and blue clusters. However, in this particular experiment, each of the samples is composed of only one phospholipid and the samples should be homogeneous, except for the samples at temperature corresponding to the phase transition temperature for a specific phospholipid. The fact that the clusters align as shown in Figure 13.8 could imply that there are "only two" environments for the Laurdan molecule; in this case, it will be the gel and the liquid crystal. However, DMPC should be in a homogeneous
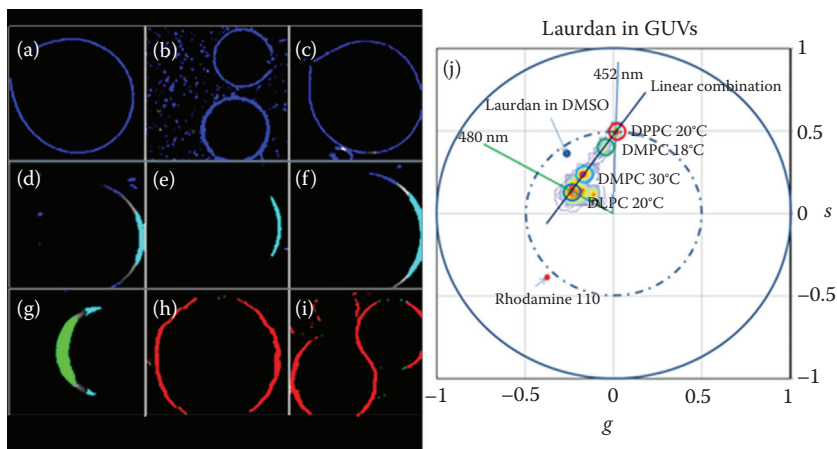
FIGURE 13.8 Spectral phasor analysis of Laurdan in GUVs made of a single phospholipid and at different temperatures. (a) DLPC at 20°C. (b and c) POPC at 20°C. (d) DMPC at 30°C. (e) DMPC at 28°C. (f) DMPC at 25°C. (g) DMPC at 21°C. (h) DMPC at 18°C. (i) DPPC at 20°C. (j) Spectral phasor plot of the GUVs samples. The underlining contour plot shows the position of the phasor for the different samples. Also, the position of the spectral phasors for Laurdan in DMSO and Rhodamine 110 in water is shown. The phasor of the GUVs apparently fall on a single line, which could be identified as the linear combination of two extreme values, for the liquid disordered phase of DLPC and DOPC at 20°C and the gel phase of DPPC at 20°C. The colors of the circles in (j) are used to paint the image with the pixels that have the phasor inside the corresponding circle in the phasor plot.

phase at least at temperatures far from the phase transition (30°C and 18°C), rather than a mixture of gel and liquid crystalline phase at all temperatures. The simplistic interpretation of the linear combination property in terms of coexistence of different phases does not hold in this case. Another possibility is that there are mainly two "environments" for the Laurdan probe, one with fast relaxation and the other with very slow relaxation, since Laurdan spectral position depends on the solvent relaxation rate. If this is the case, then the position at an intermediate value along the line between the gel and the liquid crystalline phase could just be attributed to the fraction of Laurdan molecules in the two environments. We can further elaborate on this idea and propose that the "two" environments can be identified, one with local membrane cavities with one or more molecules of water and the other with Laurdan in a tighter structure without water in the proximity. This suggestion was previously made on the basis of the observation of Laurdan spectra in a variety of conditions.[11,12]

13.5 THE LIFETIME PHASOR FOR LAURDAN IN GUVs

In regard to the lifetime, it is interesting that, in general, the lifetime of Laurdan cannot be described by only two components, but rather by a distribution of components. Depending on the emission bandwidth, the lifetime of Laurdan in the blue part of the emission spectrum is relatively long (7–8 ns) and relatively single exponential. As the

lipid composition changes, the lifetime in the blue filter aligns along the universal circle while the lifetime in the green filter could be outside of the universal circle because of the dipolar relaxation effect as the relaxation time becomes comparable in time to the overall decay time (see Figure 13.9 for an explanation why the phasor in the green filter can be outside of the universal circle).

In relation to Figure 13.9, if we measure the decay in the blue emission filter, the lifetime phasor position for Laurdan in the absence of surrounding water is shown in blue (low polarity, depending on the lipid environment). As the polarity of the medium increases, the lifetime shortens and the lifetime phasor moves along the universal circle to lower lifetime values (more polar position). The line between less polar and more polar corresponds to the linear combination of the Laurdan in the two environments, that is, to the fraction of molecules in polar versus nonpolar environments. If we measure the decay in the green emission bandpass, the unrelaxed or relaxed positions in Figure 13.9 correspond to the Laurdan molecules sensing
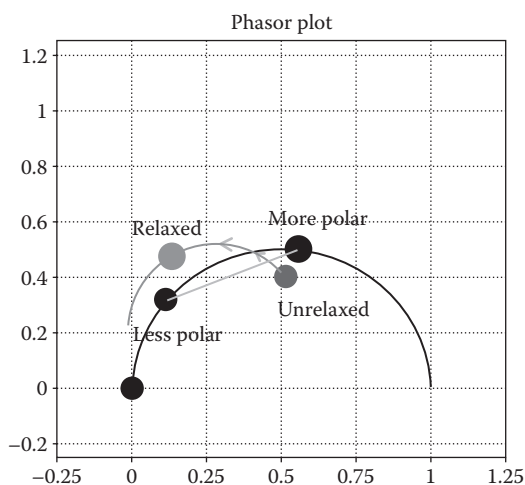

FIGURE 13.9 Schematic representation of the lifetime phasor position expected for Laurdan at two emission bandpass (gray 440/20 nm and light gray 540/40 nm, shown in black color in the figure). In the gray filter, the phasor position is on the universal circle, which indicates that Laurdan decays as a single exponential in the gray filter. The lifetime is quenched because of the polarity of the surrounding solvent. This effect should not be confused with solvent dipolar relaxation. The phasor position moves along the universal circle depending on the amount of quenching. If in one pixel there is a mixture of environments with different polarity, in this pixel, the phasor must fall in the gray line joining the two extreme values. In the light gray filter, the position of the phasor is determined by the solvent relaxation. In the absence of relaxation or if the relaxation is very fast, the position of the phasor is generally inside the universal circle owing to the heterogeneity of the decay. As the rate of dipolar relaxation increases, the phasor position moves toward the outside of the universal circle because the intensity increases with a delay with respect to the excitation. The maximum displacement toward the outside of the universal circle occurs when the rate of dipolar relaxation matches the decay rate.

different degrees of solvent dipolar relaxation. As the relaxation time increases, the phasor position in the green filter moves toward the position indicated with the dark gray toward the relaxed position (Figure 13.9). The maximum displacement along the dark gray curve is obtained when the relaxation time matches the decay time.

In Figure 13.10, we show the phasor lifetime analysis of GUVs made of a single phospholipid (DOPC and DPPC) at the same temperature (20°C) in the blue and green filters, respectively.

Figure 13.10 and the explanations given in its caption are used to construct an empirical lifetime phasor scale for the membrane fluidity. Note that the scale is very different at different wavelengths (blue vs. green) and that this scale is influenced by
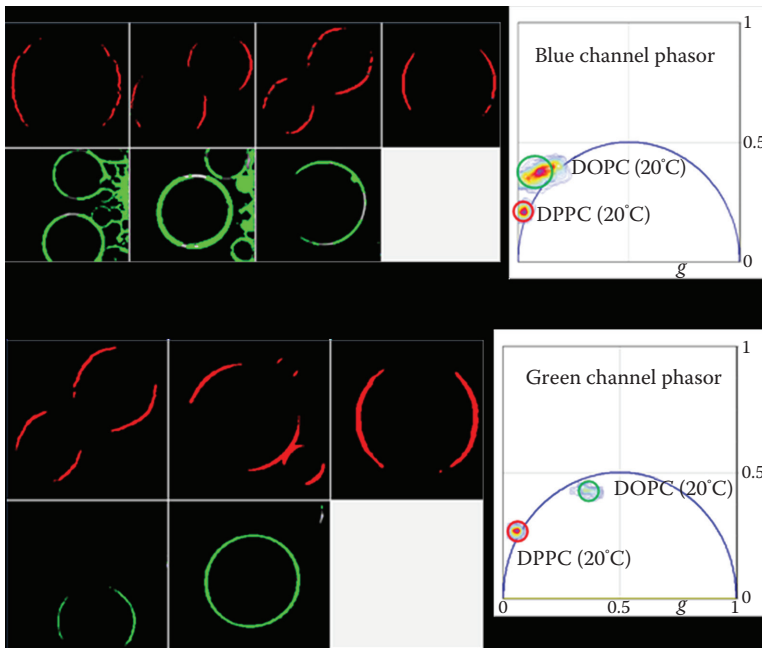

FIGURE 13.10 Empirical sensitivity scale for Laurdan lifetime phasor in two extreme phases, gel and liquid crystalline, and at two emission bandpasses (blue channel = 440/20 nm and green channel = 540/40 nm). The red cursor marks the position of the gel phase as found in the DPPC GUVs at room temperature, and the green cursor corresponds to the phasor position of DOPC at room temperature, which is in the liquid disordered phase. Excitation was obtained using a Ti:sapphire laser at 790 nm with a repetition frequency of 80 MHz. In DPPC, there are no measurable dipolar relaxations. The lifetime phasor position is largely independent of the emission wavelength. The fluorescence lifetime in this phase is approximately 8.0 ns. For DOPC, the relaxations are relatively fast and the emission in the blue channel senses the relaxations. The phasor distribution is elongated and outside the universal circle, indicating that there is lifetime heterogeneity and that the long lifetime components are sensitive to the dipolar relaxations. In the green channel, DOPC lifetime is quite short and faster than the dipolar relaxations, so that the phasor position returns inside the universal circle, according to the explanations given in Figure 13.9.

factors that change the polarity and the solvent relaxation rates. Also note that only in the green channel is the span of the fluidity scale relatively large (approximately a quarter of the phasor plot). In comparison with the spectral phasor scale in Figure 13.8, the span of the lifetime scale is reduced.

The effect of cholesterol on the spectral position and the spectral lifetime is quite interesting, and it can be understood on the basis of the spectroscopic principles outlined in the first part of this section.[13] In general, as the cholesterol concentration increases, not only does the spectrum move toward the blue, but the lifetime also becomes longer, allowing for observation of slower dipolar relaxation even in the green part of the emission spectrum. The combinations of these two effects, blue shifting but lengthening of the lifetime in the green filter, provides a characteristic signature of the presence of cholesterol. This idea has been recently presented,[13] and it is a direct consequence of the scheme shown in Figure 13.9.

As a take-home message regarding the characteristic spectroscopic properties of Laurdan, the apparent alignment of the phasors along a straight line cannot be taken as evidence that we are observing the contribution of two (or more) phases in the region of observation (pixel), but two different environments for the Laurdan molecules. Since these two (or more) environments can also be observed in phases of a single phospholipid far from the phase transition temperature, we believe that the two environments are attributed to situations in which the Laurdan molecules have no water around at the time of excitation and the other situation to Laurdan molecules with some water around. Membrane packing alone could be responsible for this effect. The same conclusion, that is, that the apparent alignment of the phasor clusters in the phasor plot does not imply that there are only two phases in the region of observation, applies to the lifetime phasor, which has a more complex behavior because the apparent lifetime is a function of the emission wavelength.

We propose, using the position along the linear combination line as a measure of water penetration, to provide an empirical scale of membrane "fluidity." To establish this empirical scale of fluidity, we measured the phasor positions of Laurdan in an artificial system composed of different lipids that at the same temperature form two different phases, liquid and gel. Of course, we do not expect these two phases to exist in biological systems, but we are using this scale as an indication of the maximum range of changes expected in lipid bilayer systems.

13.6 LIVE CELL MEMBRANE FLUIDITY

13.6.1 SPECTRAL PHASORS

A highly debated issue about biological membranes relates to the formation of membrane microdomains with specific characteristics distinct from the rest of the membranes. Since the spectrum of Laurdan reflects the water content of the membrane and, indirectly, membrane fluidity, the question arises whether it is possible, using the Laurdan probe, to distinguish different microdomains in biological membranes and characterize their size and location.

Figure 13.11 shows the phasor spectral analysis of the cancer cell line 3T3. The series of images are obtained at different z-sections spaced by 0.6 μm. The phasor distribution
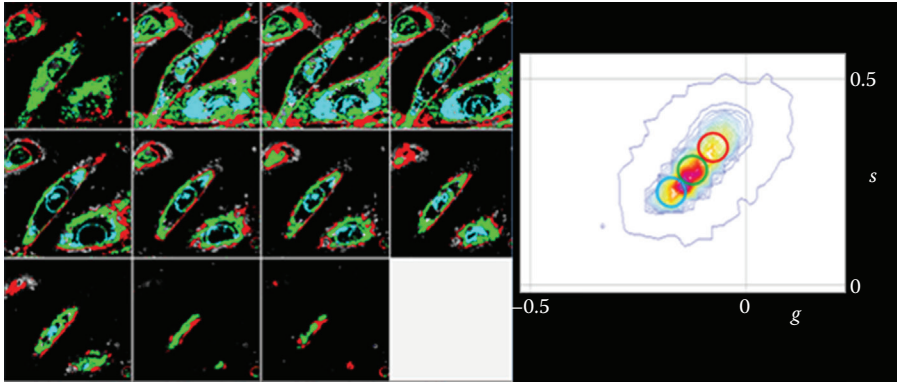
FIGURE 13.11 Z section images of 3T3 cells taken each 0.6 μm. The fluorescence was excited at 790 nm and the emission was collected using the spectral detector of the Zeiss 710LSM. In the right part of the figure, the spectral phasor plot is shown. The contour lines indicate the density of pixels with a given value of the phasor. The image on the left is colored according to the phasor position indicated with the colored circles in the phasor plot. Clearly, the phasor distribution is elongated and we can distinguish at least three different regions in the phasor plot that correspond to the plasma membrane and two regions corresponding to internal structures in the cells. The average line in this plot has a different slope from the line in Figure 13.8, indicating that the environment of the cell membrane is different from the single phospholipid environ of the GUVs used to produce Figure 13.8.

is broad and it distributes along a line, which is different from the line obtained using GUVs of different compositions. In relation to the spectra in single lipid GUVs and using the proposed empirical fluidity scale, the cell membranes corresponding to internal membranes (mitochondria, Golgi, and endoplasmic reticulum) are less packed than the plasma membrane. This observation corresponds to the common knowledge that the plasma membrane is the most rigid of the cell membranes. Instead, the spectral phasor of the plasma membrane is broader (smaller radius in Figure 13.11) than the spectrum of the gel-phase GUV. In cell membranes, the prevalent phase should be the Ld phase for the plasma membrane. Measurements of the spectral phasor of GUV composed of lipid mixture in the Lo phase (data not shown) show that the location of plasma membrane phasor is closer to the location of the Lo phase. Figure 13.12 shows higher-resolution data for the spectral phasor from a different 3T3 cell and the corresponding spectral phasor plot.

We can clearly see that the plasma membrane is relatively homogeneous and with low water content. Our measurements show that the phasor of the various membranes in a cell aligns along a common straight line, which reflects the different local environment of Laurdan in the various membranes. We could carefully examine different parts of the plasma membrane (Figure 13.12) and notice that different sections of the plasma membrane have definitely different spectra (indicated by the arrows in Figure 13.12). However, at the level of resolution of the images in these figures, it is not possible to distinguish if these regions correspond to regions where the internal membranes get closer to the plasma membrane or there are microdomains in the plasma membrane of different spectral properties.
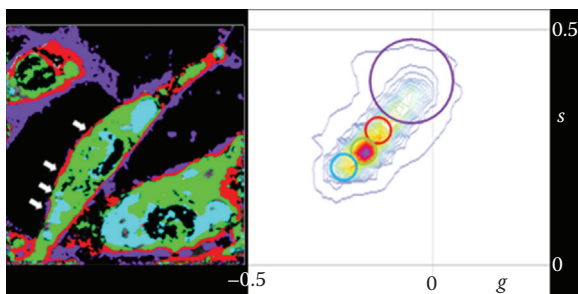
FIGURE 13.12   Single section of a 3T3 cell. The fluorescence was excited at 790 nm and the emission was collected using the spectral detector of the Zeiss 710LSM. In the right part of the figure, the spectral phasor plot is shown. The contour lines indicate the density of pixels with a given value of the phasor. The image on the left is colored according to the phasor position indicated with the colored circles in the phasor plot. As shown in Figure 13.11, the phasor distribution is elongated, and at this resolution, we can distinguish at least four different regions in the phasor plot. The violet-colored region corresponds to points with low intensity mainly at the border of the cell. The position and color coding of the other regions are the same as in Figure 13.11. Following the cell contour, we observe regions of the cell membrane indicated by white arrows with different spectra as selected by the different regions in the spectral phasor plot. This large spectral heterogeneity could indicate either that the pixels along the cell contour are contaminated by the contribution of both external and internal membranes or that the plasma membrane is made of macroscopic domains of different Laurdan spectral characteristics.

13.6.2 Lifetime Phasors in Live 3T3 Cells

The lifetime phasor analysis of 3T3 cells shows a similar behavior of the spectral phasor where the plasma membrane corresponds to higher values in our fluidity scale and the internal membranes are more fluid. Also, in this type of cells, the plasma membrane displays alternating regions of different values in the empirical fluidity scale. Figure 13.13 shows the lifetime phasor analysis in the blue and green channels. Compared to the GUVs in Figure 13.10, the location of the phasors in the blue channel is completely outside the universal circle, indicating that dipolar solvent relaxation is responsible for this effect. This observation implies that all membranes, including the plasma membrane and the internal membrane, are strongly affected by the dipolar relaxation effect. This is also shown in the green channel. As we know, dipolar relaxation is enhanced by cholesterol, which has the effect of lengthening the average lifetime and therefore better matching the decay rate with the solvent relaxation rate.

One feature of the images colored according to the phasor location is the spotted appearance of the plasma membrane. To further investigate if this spotted appearance is simply caused by noise or there is a continuation of the spots if we perform a series of three-dimensional (3D) sections, we obtained the spectral information at each section and we performed the phasor analysis at each section maintaining the selection of phasors at each section. In this way, we can obtain a 3D mask of a given color that corresponds to the empirical fluidity scale that we constructed using the data in Figures 13.11 and 13.12. The results are displayed in Figure 13.14. Figure 13.14a is the intensity
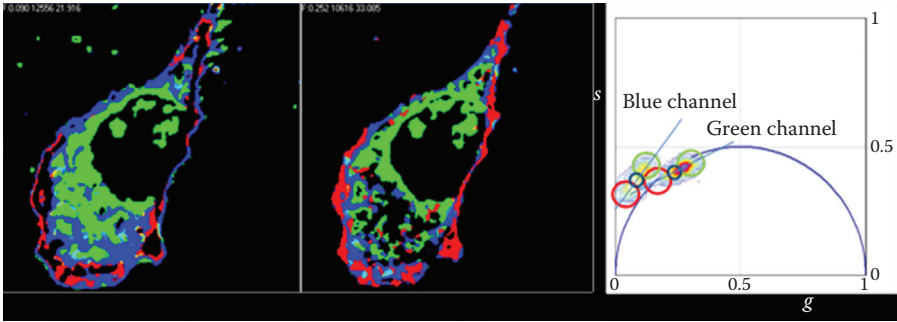
FIGURE 13.13   Lifetime phasor plot of a 3T3 cell. Excitation was at 790 nm using a Ti:sapphire laser and emission was measured at two bandpasses (440/20 nm and 540/40 nm). Images are colored according to the selection of the phasor clusters in the phasor plot. Colors are matched for the selections and the colors in the figure. The image size is 43 × 43 μm. According to the empirical fluidity scale, the plasma membrane has less fluid than the internal membrane and the contour of the cell is spotted.

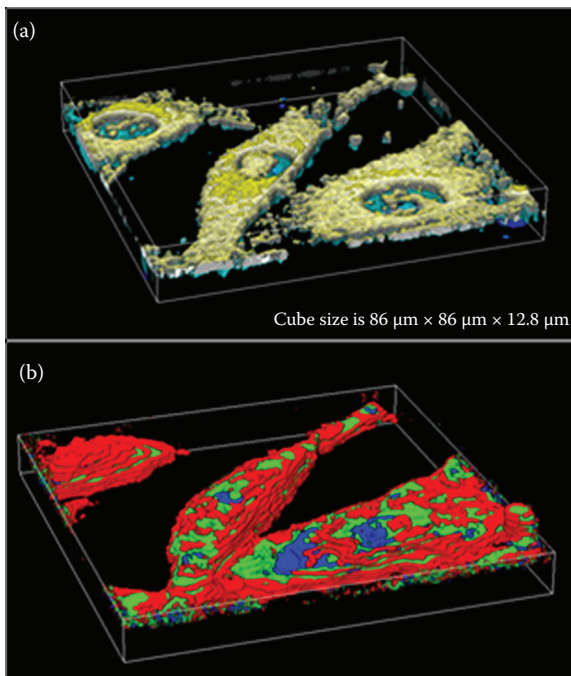**FIGURE 13.14**   3D reconstruction of intensity and spectral phasor masks of a 3T3 cell. The masks were obtained using the spectral phasor positions of Figures 13.11 and 13.12. The color code is also the same used in these figures. The 3D reconstruction shows that the appearance of spots in the contours of single sections is attributed to the large domain spectral heterogeneity of the cell membrane.

image colored according to the z-section. Figure 13.14b is the same image but colored according to the phasor mask used in Figures 13.11 and 13.12. Clearly, the entire plasma membrane appears less fluid in this 3D reconstruction and the spots observed in the single images are actually sections of much larger regions of different fluidity.

13.7 CONCLUSIONS AND FURTHER CONSIDERATIONS

In conclusion, the location of a specific phasor cluster in the line of linear combination between the Lo and Ld phases cannot be interpreted as evidence of the coexistence of microdomains in these regions but only reports the fraction of very local environments of the Laurdan molecules. These local environments correspond in our opinion to membrane defects where one or more molecules of water can reside and can produce the solvent relaxation effect, which is the signature of the shifts of the emission spectrum of Laurdan and of the apparent changes of lifetime. Unless other information about the clustering of these cavities is obtained, for example, independent measurement of the size, we cannot conclude that an intermediate position of the spectrum or lifetime between two extremes is evidence of membrane microdomains, although membrane microdomains will produce this behavior. However, an analysis of the spectral and lifetime behavior of Laurdan shows a very rich scenario where relatively large domains resolved at the diffraction-limited resolution of the experiments reported in this contribution that extend in 3D. In addition, Laurdan is clearly sensitive to the relative differences in fluidity between different internal cell membranes.

From a biological point of view, membrane fluidity changes are implicated in a range of biological processes including signaling, membrane fusion, endocytosis, and many others. For example, the role of membrane fluidity during development has been discussed,[14–23] but we are still lacking a systematic study of changes in membrane fluidity during embryo development. In general, lipids and lipid domains independent of their size play a fundamental role in the structural organization of the cytoplasmic membrane of eukaryotic cells. The results described in this chapter show that Laurdan can detect the difference between the plasma membrane and the membranes of internal organelles, which are of fundamental importance for the compartmentalization of cell functions. The complexity of the membrane lipid composition has suggested the coexistence of domains characterized by different dynamic properties in the membrane plane as sites for preferential partitioning of proteins and solutes, for modulating membrane activity, and for diffusion along the plane and through the bilayer.[24–33]

Several invasive methods that use membrane isolation can be used to establish the exact lipid composition of membranes. However, when these methods are used to study membrane domains, they can be subject to localization error because lipids can migrate between different cellular compartments during the membrane isolation. Instead, fluorescence spectroscopy can be used directly in live cells and in tissues while the cells are being excited and are functioning in their natural biological environments. Using fluorescence, the information on membrane packing and dynamics is obtained from the spectroscopic properties of fluorescent probes residing in the membrane at very low concentrations, generally less than 1:100 probe-to-lipid molar ratio.

Among several fluorescent probes, the sensitivity of Laurdan to the polarity of the membrane environment presents several advantages for membrane studies. This

sensitivity arises from the greater than 50 nm red shift of the emission maximum in polar versus nonpolar environments, so that simple fluorescence intensity measurements at two properly selected wavelengths provide information on the membrane polarity. Several studies have shown that Laurdan spectroscopic properties reflect local water content in the membrane and, indirectly, membrane fluidity. Laurdan is a molecule whose spectroscopic properties are influenced by both the composition and dynamics of its local surroundings.[2–4,11,13,34–45] In other words, Laurdan's fluorescence properties are dependent on two major factors: the polarity of the environment (ground state of the fluorophore) and the rate of dipolar relaxation of molecules or molecular residues that can reorient around Laurdan's fluorescent moiety during its excited-state lifetime.

In this chapter, we show that spectral and lifetime information can be analyzed in a common framework on the basis of the phasor transformation. This is important in the evaluation of the sensitivity of the two spectroscopic approaches. We show here that while spectral analysis has a larger range, lifetime analysis offers a possibility to distinguish unambiguously between changes in polarity and changes in the solvent dipolar relaxation rate.

In this chapter, we compare the use of Laurdan emission spectra and Laurdan fluorescence lifetime as a means to determine differences between membranes in eukaryotic cells, with particular emphasis on the membranes of cancer cell lines. We discuss the different information that can be extracted using spectral and lifetime measurements of Laurdan in live cells when these techniques are applied to confocal images. Using the spectral and the FLIM approach, we build a fluidity scale based on calibration with model systems of different lipid composition. Using FLIM, we show that it is possible to quantify and separate the changes in membrane water content that affect the spectral relaxation process of Laurdan from changes that are caused by polarity of the Laurdan environment, which mainly affect the emission spectrum. Both for the analysis of FLIM data and spectral data, we use a common approach based on the use of phasors. The phasor approach is a fit-less way to visually display where in the cells Laurdan has different spectroscopic properties. The relevance of the phasor approach is that it allows a simple graphical way to separate regions of the cells where we have coexistence of different environments from other regions where there are unique but different environments. The measurement of the phasor locations in GUVs made of single lipids of different transition temperatures allows us to construct a sensitivity scale that we can use to compare the spectral and the FLIM approach. An analysis of different membranes of the same cell shows marked differences in spectroscopic properties as well as in lifetime. These differences allow the use of a single probe to label different membranes. Since Laurdan easily diffuses in cell cultures and tissues and is not fluorescent in the aqueous environment, its use is particularly simple in biological samples.

13.8 METHODS

13.8.1 Preparation of the GUVs

Phospholipids (from Avanti Polar, Alabama) were diluted with chloroform to a final concentration of 0.2 mg/ml. Two platinum wires attached to a Teflon chamber were coated with 2 μl of the lipid mixture and dried under N_2 (g). The water-jacketed

chamber was sealed with a No. 1.5 coverslip and was attached to a circulating water bath according to the procedure from Ruan et al.[46] Phospholipids were rehydrated with 1 mM Tris, pH 7.4. The platinum wires were attached to a frequency generator with alternating current set to 10 Hz and 2 V. A thermocouple was used to monitor the temperature of the chamber.

13.8.2   NIH3T3 Cell Cultures

NIH/3T3 (mouse fibroblast) cell line was purchased from Sigma-Aldrich. The cells were cultured in Dulbecco's Modified Eagle's Medium, supplemented with 1.5 g/L sodium bicarbonate, 10 mM HEPES, pH 7.4, 100 U/mL penicillin G, 100 L/g/mL streptomycin, and 10% fetal calf serum at 37°C in a humidified atmosphere consisting of 95% air and 5% CO_2. Cells were passaged by removing 90% of the supernatant and replacing it with fresh medium approximately twice a week and detachment using a 0.25% trypsin–EDTA solution. For FLIM experiments, the cells were scraped and plated on glass bottom dishes (MatTek, AshLand, USA) coated with 10 μg/ml poly-D-lysine (MP Biomedicals, California, USA) and 20 μg/ml laminin (Sigma-Aldrich), 1 day before the analysis.

13.8.3   FLIM Analysis

FLIM data were acquired with a Zeiss LSM710 META laser scanning microscope, coupled to a 2-Photon Ti:sapphire laser (Spectra-Physics Mai Tai, Newport Beach, CA) producing 80 fs pulses at a repetition of 80 MHz and an ISS A320 FastFLIMBox (ISS Inc., Champaign, IL) for the lifetime data. A 40× water immersion objective 1.2 N.A. (Zeiss, Oberkochen, Germany) was used for all experiments. The excitation wavelength was set at 780 nm. An SP 760 nm dichroic filter was used to separate the fluorescence signal from the laser light. For FLIM data, the fluorescence signal was directed through a 495 LP filter and the signal was split between two photo-multiplier detectors (H7422P-40, Hamamatsu, Japan), with the following bandwidth filters in front of each: blue channel 460/40 and green 540/25, respectively. For image acquisition, the pixel frame size was set to 256 × 256 and the pixel dwell time was 25.61 μs/pixel. The average laser power at the sample was maintained at the milliwatt level.

13.8.4   Spectral Analysis

All images were taken using a Zeiss LSM710 spectral emission microscope equipped with a two-photon laser. Laurdan was excited at 780 nm and the spectral emission was collected at 9.4 nm bands centered between 421 and 723 nm. Each data set was collected at 256 × 256 pixels at 177 μs/pixel. For cell work, 3D z-stacks were taken at 1 μm or 0.6 μm z-section steps (range, between 20 and 40 slices).

ACKNOWLEDGMENT

REFERENCES

1. Weber, G., and F. J. Farris. "Synthesis and Spectral Properties of a Hydrophobic Fluorescent Probe: 6-Propionyl-2-(Dimethylamino)Naphthalene." *Biochemistry* 18, no. 14 (1979): 3075–8.

2. Parasassi, T., G. De Stasio, A. d'Ubaldo, and E. Gratton. "Phase Fluctuation in Phospholipid Membranes Revealed by Laurdan Fluorescence." *Biophys J* 57, no. 6 (1990): 1179–86.

3. Parasassi, T., G. De Stasio, G. Ravagnan, R. M. Rusch, and E. Gratton. "Quantitation of Lipid Phases in Phospholipid Vesicles by the Generalized Polarization of Laurdan Fluorescence." *Biophys J* 60, no. 1 (1991): 179–89.

4. Parasassi, T., E. Gratton, W. M. Yu, P. Wilson, and M. Levi. "Two-Photon Fluorescence Microscopy of Laurdan Generalized Polarization Domains in Model and Natural Membranes." *Biophys J* 72, no. 6 (1997): 2413–29.

5. Bagatolli, L. A., and E. Gratton. "Two Photon Fluorescence Microscopy of Coexisting Lipid Domains in Giant Unilamellar Vesicles of Binary Phospholipid Mixtures." *Biophys J* 78, no. 1 (2000): 290–305.

6. Bagatolli, L. A. "Direct Observation of Lipid Domains in Free Standing Bilayers: From Simple to Complex Lipid Mixtures." *Chem Phys Lipids* 122, no. 1–2 (2003): 137–45.

7. Digman, M. A., V. R. Caiolfa, M. Zamai, and E. Gratton. "The Phasor Approach to Fluorescence Lifetime Imaging Analysis." *Biophys J* 94, no. 2 (2008): L14–6.

8. James, N. G., J. A. Ross, M. Stefl, and D. M. Jameson. "Applications of Phasor Plots to In Vitro Protein Studies." *Anal Biochem* 410, no. 1 (2011): 70–6.

9. Jameson, D. M., E. Gratton, and R. Hall. "The Measurement and Analysis of Heterogeneous Emissions by Multifrequency Phase and Modulation Fluorometry." *Appl Spectrosc Rev* 20, no. 1 (1984): 55–106.

10. Fereidouni, F., A. N. Bader, and H. C. Gerritsen. "Spectral Phasor Analysis Allows Rapid and Reliable Unmixing of Fluorescence Microscopy Spectral Images." *Opt Express* 20, no. 12 (2012): 12729–41.

11. Bagatolli, L. A., E. Gratton, and G. D. Fidelio. "Water Dynamics in Glycosphingolipid Aggregates Studied by Laurdan Fluorescence." *Biophys J* 75, no. 1 (1998): 331–41.

12. Bagatolli, L. A., T. Parasassi, G. D. Fidelio, and E. Gratton. "A Model for the Interaction of 6-Lauroyl-2-(N,N-Dimethylamino)Naphthalene with Lipid Environments: Implications for Spectral Properties." *Photochem Photobiol* 70, no. 4 (1999): 557–64.

13. Golfetto, O., E. Hinde, and E. Gratton. "Laurdan Fluorescence Lifetime Discriminates Cholesterol Content from Changes in Fluidity in Living Cell Membranes." *Biophys J* 104, no. 6 (2013): 1238–47.

14. Los, D. A., K. S. Mironov, and S. I. Allakhverdiev. "Regulatory Role of Membrane Fluidity in Gene Expression and Physiological Functions." *Photosynth Res* 116, no. 2–3 (2013): 489–509.

15. Lin, C., L. H. Wang, T. Y. Fan, and F. W. Kuo. "Lipid Content and Composition During the Oocyte Development of Two Gorgonian Coral Species in Relation to Low Temperature Preservation." *PLoS One* 7, no. 7 (2012): e38689.

16. Marguet, D., P. F. Lenne, H. Rigneault, and H. T. He. "Dynamics in the Plasma Membrane: How to Combine Fluidity and Order." *EMBO J* 25, no. 15 (2006): 3446–57.

17. Nozawa, Y., R. Kasai, Y. Kameyama, and K. Ohki. "Age-Dependent Modifications in Membrane Lipids: Lipid Composition, Fluidity and Palmitoyl-CoA Desaturase in Tetrahymena Membranes." *Biochim Biophys Acta* 599, no. 1 (1980): 232–45.

18. Quinn, P. J., and D. Chapman. "The Dynamics of Membrane Structure." *CRC Crit Rev Biochem* 8, no. 1 (1980): 1–117.

19. Wang, T. Y., and J. R. Silvius. "Sphingolipid Partitioning into Ordered Domains in Cholesterol-Free and Cholesterol-Containing Lipid Bilayers." *Biophys J* 84, no. 1 (2003): 367–78.

20. Weeks, G., and F. G. Herring. "The Lipid Composition and Membrane Fluidity of Dictyostelium Discoideum Plasma Membranes at Various Stages During Differentiation." *J Lipid Res* 21, no. 6 (1980): 681–6.

21. Wisniewska, A., J. Draus, and W. K. Subczynski. "Is a Fluid-Mosaic Model of Biological Membranes Fully Relevant? Studies on Lipid Organization in Model and Biological Membranes." *Cell Mol Biol Lett* 8, no. 1 (2003): 147–59.

22. Hashimoto, M., S. Hossain, and S. Masumura. "Effect of Aging on Plasma Membrane Fluidity of Rat Aortic Endothelial Cells." *Exp Gerontol* 34, no. 5 (1999): 687–98.

23. Hitzemann, R. J., and D. A. Johnson. "Developmental Changes in Synaptic Membrane Lipid Composition and Fluidity." *Neurochem Res* 8, no. 2 (1983): 121–31.

24. Ayuyan, A. G., and F. S. Cohen. "Raft Composition at Physiological Temperature and pH in the Absence of Detergents." *Biophys J* 94, no. 7 (2008): 2654–66.

25. Bakht, O., P. Pathak, and E. London. "Effect of the Structure of Lipids Favoring Disordered Domain Formation on the Stability of Cholesterol-Containing Ordered Domains (Lipid Rafts): Identification of Multiple Raft-Stabilization Mechanisms." *Biophys J* 93, no. 12 (2007): 4307–18.

26. Fan, J., M. Sammalkorpi, and M. Haataja. "Lipid Microdomains: Structural Correlations, Fluctuations, and Formation Mechanisms." *Phys Rev Lett* 104, no. 11 (2010): 118101.

27. Gallegos, A. M., S. M. Storey, A. B. Kier, F. Schroeder, and J. M. Ball. "Structure and Cholesterol Dynamics of Caveolae/Raft and Nonraft Plasma Membrane Domains." *Biochemistry* 45, no. 39 (2006): 12100–16.

28. Martinez-Seara, H., T. Rog, M. Pasenkiewicz-Gierula et al. "Interplay of Unsaturated Phospholipids and Cholesterol in Membranes: Effect of the Double-Bond Position." *Biophys J* 95, no. 7 (2008): 3295–305.

29. Maurya, S. R., D. Chaturvedi, and R. Mahalakshmi. "Modulating Lipid Dynamics and Membrane Fluidity to Drive Rapid Folding of a Transmembrane Barrel." *Sci Rep* 3 (2013): 1989.

30. Niemela, P. S., S. Ollila, M. T. Hyvonen, M. Karttunen, and I. Vattulainen. "Assessing the Nature of Lipid Raft Membranes." *PLoS Comput Biol* 3, no. 2 (2007): e34.

31. Sengupta, P., B. Baird, and D. Holowka. "Lipid Rafts, Fluid/Fluid Phase Separation, and Their Relevance to Plasma Membrane Structure and Function." *Semin Cell Dev Biol* 18, no. 5 (2007): 583–90.

32. Wassall, S. R., M. R. Brzustowicz, S. R. Shaikh et al. "Order from Disorder, Corralling Cholesterol with Chaotic Lipids. The Role of Polyunsaturated Lipids in Membrane Raft Formation." *Chem Phys Lipids* 132, no. 1 (2004): 79–88.

33. Kusumi, A., and K. Suzuki. "Toward Understanding the Dynamics of Membrane-Raft-Based Molecular Interactions." *Biochim Biophys Acta* 1746, no. 3 (2005): 234–51.

34. Sanchez, S. A., M. A. Tricerri, and E. Gratton. "Laurdan Generalized Polarization Fluctuations Measures Membrane Packing Micro-Heterogeneity In Vivo." *Proc Natl Acad Sci U S A* 109, no. 19 (2012): 7314–9.

35. Bagatolli, L. A., S. A. Sanchez, T. Hazlett, and E. Gratton. "Giant Vesicles, Laurdan, and Two-Photon Fluorescence Microscopy: Evidence of Lipid Lateral Separation in Bilayers." *Methods Enzymol* 360 (2003): 481–500.

36. Parasassi, T., and E. Gratton. "Membrane Lipid Domains and Dynamics as Detected by Laurdan Fluorescence." *J Fluoresc* 5, no. 1 (1995): 59–69.

37. Parasassi, T., M. Di Stefano, M. Loiero, G. Ravagnan, and E. Gratton. "Cholesterol Modifies Water Concentration and Dynamics in Phospholipid Bilayers: A Fluorescence Study Using Laurdan Probe." *Biophys J* 66, no. 3 Pt 1 (1994): 763–8.

38. Kantar, A., P. L. Giorgi, E. Gratton, and R. Fiorini. "Probing the Interaction of Paf with Human Platelet Membrane Using the Fluorescent Probe Laurdan." *Platelets* 5, no. 3 (1994): 145–8.

39. Parasassi, T., M. Di Stefano, M. Loiero, G. Ravagnan, and E. Gratton. "Influence of Cholesterol on Phospholipid Bilayers Phase Domains as Detected by Laurdan Fluorescence." *Biophys J* 66, no. 1 (1994): 120–32.

40. Fiorini, R., G. Curatola, A. Kantar, P. L. Giorgi, and E. Gratton. "Use of Laurdan Fluorescence in Studying Plasma Membrane Organization of Polymorphonuclear Leukocytes During the Respiratory Burst." *Photochem Photobiol* 57, no. 3 (1993): 438–41.

41. Levi, M., P. V. Wilson, O. J. Cooper, and E. Gratton. "Lipid Phases in Renal Brush Border Membranes Revealed by Laurdan Fluorescence." *Photochem Photobiol* 57, no. 3 (1993): 420–5.

42. Parasassi, T., G. Ravagnan, R. M. Rusch, and E. Gratton. "Modulation and Dynamics of Phase Properties in Phospholipid Mixtures Detected by Laurdan Fluorescence." *Photochem Photobiol* 57, no. 3 (1993): 403–10.

43. Parasassi, T., M. Di Stefano, G. Ravagnan, O. Sapora, and E. Gratton. "Membrane Aging During Cell Growth Ascertained by Laurdan Generalized Polarization." *Exp Cell Res* 202, no. 2 (1992): 432–9.

44. Parasassi, T., and E. Gratton. "Packing of Phospholipid Vesicles Studied by Oxygen Quenching of Laurdan Fluorescence." *J Fluoresc* 2, no. 3 (1992): 167–74.

45. Parasassi, T., F. Conti, and E. Gratton. "Time-Resolved Fluorescence Emission Spectra of Laurdan in Phospholipid Vesicles by Multifrequency Phase and Modulation Fluorometry." *Cell Mol Biol* 32, no. 1 (1986): 103–8.

46. Ruan, Q., M.A. Cheng, M. Levi, E. Gratton, and W. Mantulin. "Spatial-temporal studies of membrane dynamics: Scanning fluorescence correlation spectroscopy (SFCS)." Biophys J 87, no. 2 (2004): pp. 1260–1267. doi: 10.1529/biophysj.103.036483 PMCID: PMC1304464.